Functional organization of three-dimensional orientation encoding within the visual cortex

Reuben Rideaux & Andrew E Welchman
Department of Psychology, Downing Street, University of Cambridge, CB2 3EB, UK
reuben.rideaux@gmail.com

ABSTRACT

Visual perception of three-dimensional structure is important for object recognition, grasping, and manipulation. The three-dimensional structure of a surface can be defined in terms of its slant and tilt. Previous work has shown that slant and tilt are represented in the posterior and ventral intraparietal sulcus of the human brain; however, it is unclear whether the representation of these features is functionally organized within this region. Here we use phase-encoded presentation of 3-D planar surfaces with linear gradients defined by horizontal binocular disparity while measuring fMRI activity to test whether the representation of 3-D orientation, both for slant and tilt, is functionally organized within the visual cortex. We find functionally defined structures within V3A and V7 for both slant and tilt. Most notably, in two participants we find that the tilt preference is unilaterally organized in a pinwheel-like structure, similar to those observed for orientation preference in V1, which encompasses most of area V3A. These findings indicate that 3-D orientation is functionally organized within the human visual cortex, and the evidence suggesting the presence of a large pinwheel-like structure indicates that this type of organization may be applied canonically within the brain at multiple scales.

INTRODUCTION

Visual perception of three-dimensional (3-D) structure is important for object recognition, grasping, and manipulation. There are multiple visual cues from which 3-D structure can be inferred (e.g., texture, shading, and perspective), but arguably the most powerful cue is that provided by binocular disparity (i.e., the horizontal offset between the images seen by the left and right eyes). Considerable imaging work has progressed our understanding of where absolute and relative binocular disparity information is processed in the human brain (Backus, Fleet, Parker, & Heeger, 2001; Goncalves et al., 2015; Neri, Bridge, & Heeger, 2004; Preston, Li, Kourtzi, & Welchman, 2008; Tsao et al., 2003; Tyler, Likova, Kontsevich, & Wade, 2006); however, less is known about the regions that encode 3-D orientation (parameterized here as slant and tilt).

Electrophysiological work has identified areas in monkey cortex that contain populations of neurons tuned to 3-D orientation defined by binocular disparity, including the caudal bank of intraparietal sulcus (CIP; Rosenberg & Angelaki, 2014; Rosenberg, Cowan, & Angelaki, 2013; Taira, Tsutsui, Jiang, Yara, & Sakata, 2017) and middle temporal area (MT; Nguyenkim & DeAngelis, 2003). These neurons in jointly encode slant and tilt; however, whereas the response of neurons in CIP to slant and tilt is co-dependent (Rosenberg et al., 2013), these dimensions appear to be encoded separably in MT (Nguyenkim & DeAngelis, 2003). This work has revealed how 3-D orientation is encoded at the single-cell level, but the nature of the technique precludes identification of population level trends such as functional organization within these areas. Further, notable differences between monkey and human brain organization in relation to the representation of 3-D orientation restricts the application of these findings to human perception (Vanduffel et al., 2002).

Functional MRI work with humans has shown that the posterior and ventral intraparietal sulcus (PIPS/V3A & VIPS/V7, respectively) encode depth structure from binocular disparity (Ban & Welchman, 2015; Durand, Peeters, Norman, Todd, & Orban, 2009; Georgieva, Peeters, Kolster, Todd, & Orban, 2009). These areas have also been implicated in processing 3-D orientation defined by motion (Murray, Olshausen, & Woods, 2003; Orban, Sunaert, Todd, Van Hecke, & Marchal, 1999; Vanduffel et al., 2002), texture (Shikata et al., 2017), and shading (Tsutsui, Jiang, Yara, Sakata, & Taira, 2001). Thus far, the study of how 3-D orientation is represented within the human brain has been limited to identification of regions through contrasting (2) patterns of fMRI activation. This technique has been successfully applied in the identification of brain areas that encode 3-D orientation, but cannot reveal whether the information encoded in these areas is functionally organized.

Here we use phase-encoded presentation of 3-D stimuli while measuring fMRI activity of four human participants to test whether the representation of 3-D orientation, both for slant and tilt, is functionally organized within the visual cortex. We find functionally defined structures within V3A and V7 for both slant and tilt. Most notably, in two participants we find that the tilt preference is unilaterally organized in a pinwheel-like structure, similar to those observed for orientation preference in V1 (Blasdel, 1992; Bonhoeffer & Grinvald, 1991), that encompasses most of area V3A. Further, for two participants we find an abrupt reversal in tilt preference reversal at the (retinotopically defined) border between V3A and V7. These findings indicate that 3-D orientation is functionally organized within the human visual cortex, and evidence suggesting the presence of a large pinwheel-like structure indicates that this type of organization may be applied canonically within the brain at multiple scales.

METHODS

Participants. Four healthy participants from the University of Cambridge with normal or corrected-to-normal vision participated in the experiment. With the exception of participant 1 (author RR), participants were naïve to the aims of the experiment. The participants ages were 30, 28, 21, and 29, respectively; all were right handed and participant 3 was female. Participants were screened for stereoacuity using a discrimination task in which they judged the (near/far) depth profile of a RDS depicting an annulus surrounding a disk. The difference in depth between the annulus and disk was controlled using a 2-down 1-up staircase procedure and participants were admitted into the experiment if they achieved a threshold of <1° arcmin. Participants were also screened for contraindications to MRI prior to the experiment. All experiments were conducted in accordance with the ethical guidelines of the Declaration of Helsinki and were approved by the University of Cambridge STEM and all participants provided informed consent.

Apparatus and stimuli. Stimuli were programmed and presented in MATLAB (The MathWorks, Natick, MA) with Psychophysics Toolbox extensions (Brainard, 1997; Pelli, 1997). Stereoscopic presentation in the scanner was achieved using a "PROPixx" DLP LED projector (VPixx Technologies) with a refresh rate of 120 Hz and resolution of 1920 × 1080, operating in RB3-D mode. The left and right images were separated by a fast-switching circular polarization modulator in front of the projector lens (DepthQ; Lightspeed Design). The onset of each orthogonal polarization was synchronized with the video refresh, enabling interleaved rates of 60 Hz for each eye's image. MR-safe circular polarization filter glasses were worn by participants in the scanner to dissociate the left and right eye's view of the image. Stimuli were back-projected onto a polarization-preserving screen (Stewart Filmscreen, model 150) inside the bore of the magnet and viewed via a front-surfaced mirror attached to the head coil and angled at 45° above the participants' heads. This resulted in a viewing distance of 72 cm, from which all stimuli were visible within the binocular field of view. Stereoscopic presentation out of the scanner was achieved using a pair of Samsung 2233RZ LCD monitors (120 Hz, 1680×1050) viewed through mirrors in a Wheatstone stereoscope configuration. The viewing distance was 50 cm and participants' head position was stabilized using an eye mask, head rest and chin rest. Eye movement was recorded binocularly at 1 kHz using an EyeLink 1000 (SR Research Ltd., Ontario, Canada).

Stimuli consisted of random-dot stereograms (RDS) presented within an annulus (inner radius, .45°; outer radius, 9°) aperture on a midgray background surrounded by pink noise intended to facilitate stable vergence. The outer edge of the annulus was blurred according to a cosine profile. Dots in the stereogram followed a black or white Gaussian luminance profile, subtending 0.17° at half maximum. There were 12 dots/deg^2, resulting in ~85% coverage of the background. Dots were allowed to overlap and where this occurred they occluded previously positioned dots. Dots presented to the left and right eyes were offset to generate planar surfaces with linear gradients of horizontal disparity (**Fig. 1a**). Binocular disparity was calculated from the cyclopean view and applied to each vertex/dot based on the specific disparity-defined slant/tilt angle. In the centre of the annulus, we presented a fixation square (side length = 0.5°) paired with horizontal and vertical lines.

Psychophysics procedure. We measured participants' sensitivity to change in the slant (i.e., around the x-axis) and tilt (at 60° slant) of the stimulus with a two-interval forced-choice experimental design in which the reference and test stimuli were presented in randomized

order. The angular difference between test and reference stimulus was varied using the QUEST adaptive staircase method. Each stimulus was presented for 500 ms with an inter-stimulus interval of 500 ms. Observers indicated which stimulus was either more slanted (slant condition) or more clockwise (tilt condition) using a keypress. For slant, we measured sensitivity to change around nine reference angles from ±60° in evenly spaced increments. For tilt, we measured sensitivity to change around the four cardinal and four oblique angles. For each reference angle, we ran two randomly interleaved staircases, one that measured sensitivity to change in the positive direction and one that measured sensitivity to change in the negative direction; the final threshold estimate was derived from the average of the two staircases. Each staircase consisted of between 30 to 90 trials, depending on the number of trials required to reach a stable estimate. The order of reference angles tested for slant and tilt was randomized for each participant.

Observers could theoretically discriminate surface angle based only on the difference in depth at the edges (e.g., top and bottom) of a pair of stimuli. To minimize the availability of this cue, disparity-defined position was randomized by shifting the surface relative to the fixation plane (0° disparity) to between ±10% of the total surface depth.

Travelling wave procedure. We ran two conditions; one in which the tilt angle of the plane was held constant at 0° and the slant angle was varied between ±60° in 19 evenly spaced increments (slant condition; i.e., the plane was slanted about the x-axis; **Fig. 1b,** left), and the other in which the slant angle was held constant 60° and we varied the tilt angle of the plane between 0-360° in 24 evenly spaced increments (tilt condition; **Fig. 1b,** right). A constant binocular disparity offset (-3 arcmin) was applied to stimuli in the slant condition so that the stimulus did not align with the background at any of the slant angles presented (i.e., zero slant).

A travelling-wave paradigm was designed to generate a traveling wave of activity across/within areas representing 3-D orientation in the visual cortex. This involved presenting planar surfaces which consecutively varied in slant/tilt in either a forwards (positive to negative slant, clockwise tilt) or backwards order (negative to positive slant, counter clockwise tilt). Planar surfaces at each slant/tilt were presented for 2 s, with stimuli presented for 0.4 s separated by 0.1 s inter-stimulus-intervals consisting of only the background and fixation cross (gaps were used to reduce adaptation). A 10 s blank period separated presentation of the first and last planar surface in the slant condition (e.g., a -60° slanted plane and a 60° slanted plane), whereas in the tilt condition presentation was continuous. Each cycle of stimulation lasted 48 s. fMRI runs consisted of 7 cycles in addition to a 16 s blank interval at the beginning and end of the run, thus taking 368 s. Each participant completed two experimental scanning sessions, which consisted of eight runs (four forwards and four backwards) and lasted approximately 60 min. Participant 1 (author RR) completed two additional sessions in the slant condition (run length, 4 and 12) and one additional session in the tilt condition, and participant 2 completed an additional session in the slant condition. These additional sessions were combined in the main analysis.

During the stimulus presentation, participants performed an attentionally demanding ring detection task. This served to ensured consistent attentional allocation on the stimulus during the experiment. Participants were instructed to fixate a central crosshair fixation marker and press a button when they detected a ring. Rings consisted of annular regions (width, 0.6°) of the stimulus, centred on fixation, that were reduced in contrast by 40%, presented at one of four possible eccentricities [1.8, 3.6, 5.4, 7.2]°. The shape of the ring presented to the left and right eyes was distorted to match the 3-D orientation of the current

planar surface. Rings were presented for the duration of the stimulus presentation (0.4 s) on 5% of presentations (selected pseudorandomly).

The method used to present images stereoscopically in the scanner prohibited eye tracking, so to assess eye movements in response to the stimuli we had participants complete four runs (two backwards, two forwards) of the travelling wave paradigm outside the scanner for each (slant/tilt) condition while we monitored their eye position.

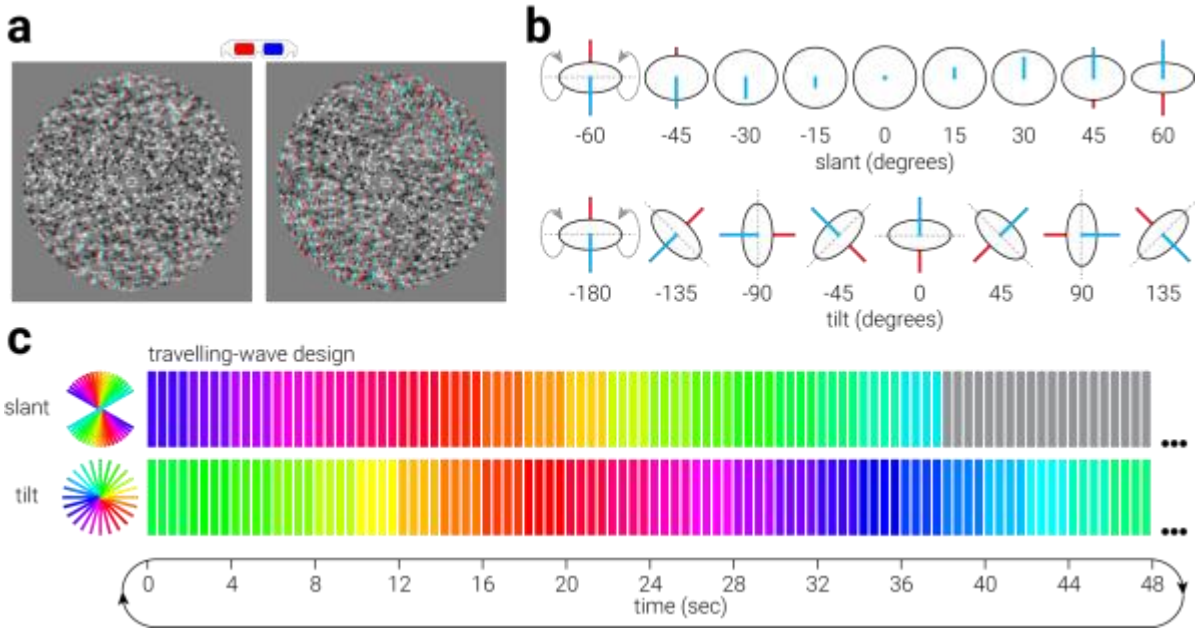

Figure 1. Three-dimensional stimuli and travelling wave procedure. a) Example random-dot stereogram stimuli used in the experiment. The image on the left shows a stimulus from the slant condition (slant , -40°; tilt 0°) and the image on the right shows a stimulus from the tilt condition (slant , -60°; tilt 45°). **b**) Illustration of varying the slant (top) and tilt (bottom) of a planar surface. **c**) Schematic diagram of travelling wave experimental design. A single cycle is shown for slant (top) and tilt (bottom) conditions, 7 cycles were repeated per run. Grey bars in the slant condition indicate periods of fixation.

Magnetic resonance imaging. Data were collected at the Wolfson Brain Imaging Center with a 3T Siemens PRISMA system using a 32-channel head coil. Blood oxygen level-dependent (BOLD) functional data were acquired with a gradient echo-planar imaging (EPI) sequence [echo time (TE) 29 ms; repetition time (TR) 2000 ms; voxel size 1.5 × 1.5 × 2 mm, 30 slices covering occipital cortex] for experimental and localizer scans. Slice orientation was near to coronal section but rotated about the mediolateral axis with the ventral edge of the volume more anterior in order to ensure coverage of lateral occipital cortex (**Fig. 2a**). A T1-weighted, 3D-MPRAGE pulse sequence, anatomical scan (voxel size 1 mm isotropic) was additionally acquired for each participant. These anatomical scans were used to register the functional data across scanning sessions, restrict the analysis of BOLD activity to gray matter voxels, and create flattened surfaces on which cortical activity is visualized.

Data processing. Anatomical scans were aligned along the ACPC plane, gray matter and white matter were segmented, and flattened surfaces were computationally rendered with BrainVoyager QX (BrainInnovation, Maastricht, The Netherlands; **Fig. 2b**). Flattened surfaces (flat maps) were rendered such that areas that were concave on the original surface (i.e., sulci) are dark gray, and areas that were convex (i.e., gyri) are light gray. Functional data were preprocessed with slice timing correction, head motion correction, and high-pass filtering before being aligned to the participant's anatomical scan. Functional

images from the first run within a session were manually aligned to the anatomical, and these alignment coordinates were used to align the images from the remaining runs. Analysis of functional imaging data was performed in MATLAB (MathWorks, Natick, MA) using in house scripts.

To evaluate periodic responses to 3D orientation, the data were analysed using a Fourier transformation-based method, well documented in the standard retinotopy studies (DeYoe et al., 1996; Engel et al., 1994; Sereno et al., 1995). As previously described by (Ban et al., 2013), forwards and backwards run time series were concatenated and a discrete Fourier transformation was computed for each voxel after converting the raw signals to percentage signal changes. The phase measurement computed from this analysis was averaged between backwards runs was reversed before being averaged with data from the forwards runs to remove the effect of the hemodynamic delay in deriving the 3-D orientation maps. Then, statistical testing to estimate the significance of correlation of BOLD signal at the stimulus frequency (1/48 Hz) was performed by comparing the squared amplitude at the stimulus frequency with the sum of squared amplitudes at the other frequencies, which yielded an *F*-ratio. The *F*-ratio was converted to a *P* value considering degrees of freedom of the signals (number of time points). In mapping retinotopic responses on the cortical surface, the polar angle phase of each significantly activated voxel was displayed using a continuous colour scale. We used a voxel-level Fourier *F*-statistic value ($F(2, \text{number of time points}) > 7.38$ and $p < 0.05$) as a criteria of significance for all Fourier-based analysis. Additionally, coherence values were obtained by calculating the voxel-by-voxel correlation between the concatenated time series and the corresponding best-fitting sinusoid at the frequency of the visual stimulation; coherence values were averaged between forwards and backwards runs. The coherence measures signal-to-noise (Engel et al., 1994; Schluppeck, 2005), and ranges from 0 to 1, where values near 1 indicate the fMRI signal modulation at the stimulus period is large relative to the noise (at the other frequency components) and values near 0 indicate that there is no signal modulation or that the signal is small compared with noise.

***Retinotopy*.** In a separate session, we performed ROI localization for each participant using retinotopic and stimulus contrast mapping procedures; the details of which are reproduced from (Murphy, Ban, & Welchman, 2013). Retinotopically organized visual areas (V1, V2, V3v, V4, V3-D, V3A, V3B/KO, and V7) were defined using polar (**Fig. 2c**) and eccentricity maps (**Fig. 2-D**), which were derived from fMRI responses to rotating wedge and expanding concentric ring stimulus presentations, respectively (DeYoe et al., 1996; Sereno et al., 1995). Area V3 was separated into ventral and dorsal quadrants in each hemisphere (V3v/d) consistent with previous delineation based on functional and cytoarchitectonic differences (Wilms et al., 2010). V4 was defined as the ventral region of visual cortex adjacent to V3v comprising a representation of the upper quadrant of the contralateral visual field (Tootell, 2001; Tyler et al., 2005). V7 was defined as the region of retinotopic activity dorsal and anterior to V3A (Tootell, 2001; Tsao et al., 2003; Tyler et al., 2005). V3B/KO (Tyler et al., 2006; Zeki, Perry, & Bartels, 2003) was defined as the area containing the union of retinotopically mapped V3B and the kinetic occipital region (KO), which was functionally localized by its preference for motion-defined boundaries compared with transparent motion of white and black dots (Dupont et al., 1997; Tootell, 2001; Tyler et al., 2006; Zeki et al., 2003). This area contained a full hemifield representation, inferior to V7 and lateral to, and sharing a foveal confluence with, V3A (Tyler et al., 2005). Human middle temporal complex (hMT+/V5) was defined as the set of voxels in lateral temporal cortex that responded significantly more strongly to transparent dot motion compared with a static array of dots

(Zeki et al., 1991). Lateral occipital complex (LOC) was defined as voxels in the lateral occipito-temporal cortex that preferred intact, compared with scrambled, images of objects (Kourtzi, Betts, Sarkheil, & Welchman, 2005). LOC subregion LO was defined based on overlap of anatomical structures and functional activations, in line with previous work (Grill-Spector, Kushnir, Hendler, & Malach, 2000).

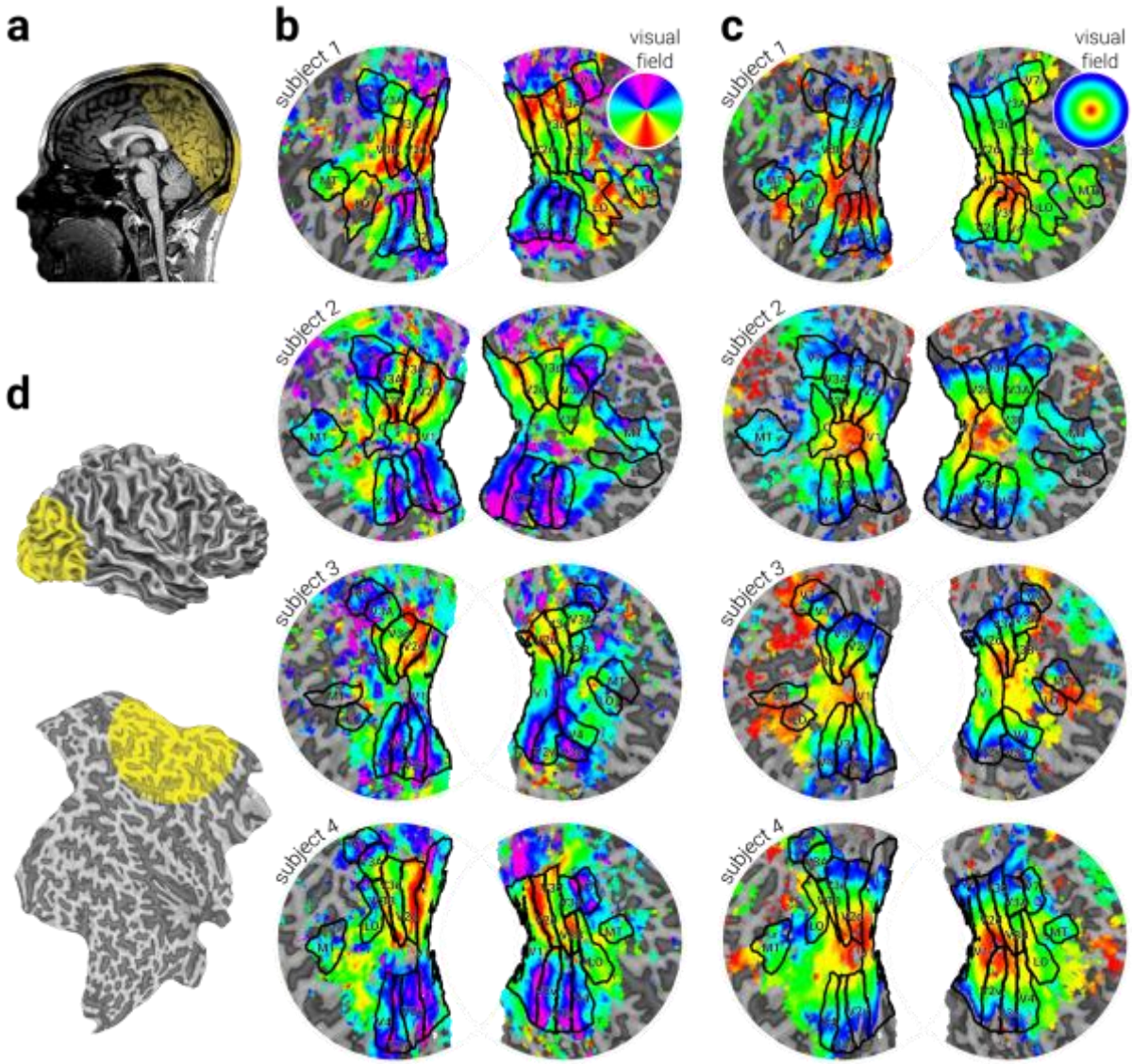

Figure 2. Retinotopic maps. a) Sagittal view of a structural MRI scan of participant 1, with coloured overlay illustrating slice orientation for functional scans. **b**) Reconstruction and flattened surface of structural scan, with coloured overlay illustrating circular regions shown in (**c-d**). (**c-d**) Flattened structural surfaces with coloured overlay illustrating phase map in response to **c**) a rotating wedge and **d**) expanding/contracting concentric rings. Black lines in (**c-d**) indicate retinotopic area demarcation.

RESULTS

***Representation of slant*.** Following retinotopic mapping of visual areas (**Fig. 2c-d**) we measured participants' phase-encoded responses to 3-D slant around the x-axis between ±60°, defined by binocular disparity. **Figure 3a** shows the coherence of the activity measured from the visual cortex with the frequency of the travelling wave stimulus. There is a high degree of coherence within all retinoptopically defined visual areas (i.e., V1, V2-D, V3-D, V3A, V3B, V7, V2v, V3v, MT, and LO), suggesting that the neural populations within these regions were sensitive to aspects of the stimulus which varied as a function of slant. **Figure 3b** shows the corresponding phase maps for each participant, which were been thresholded to remove phase values with P>.05 and those corresponding to the 10 s inter-cycle fixation period. We found a clear dominance of phase values corresponding to frontoparallel slant (i.e., 0°; **Fig. 4a**), which mirrored the results from the behavioural experiment showing participants were most sensitive to changes in slant around frontoparallel (**Fig. 4b**).

Previous work has identified areas V3A, V7, and MT as regions in which 3-D orientation is encoded (Ban & Welchman, 2015; Durand et al., 2009; Georgieva et al., 2009; Nguyenkim & DeAngelis, 2003). We reasoned that visual areas integral to encoding slant would show selectivity to a variety of slant angles. Thus, to assess the heterogeneity of slant encoding, we calculated the variability of voxel phase preference within each visual area (**Fig. 3a**, right). In line with previous work, we found that areas V3A, V7, and MT had more heterogeneous slant preference than the other visual areas; we also found that area LO had more heterogeneous slant preference than the other visual areas. The average coherence (**Fig. 4c**) and phase variability (**Fig. 4d**) across the four participants further suggested that areas V3A and V7 played an intrinsic role in supporting slant encoding. A possible concern is that patterns of activity may have been influenced by eye movements during stimulus presentation. However, we found no evidence for this; in a separate session outside the scanner in which participants performed the same task, we found binocular eye movements were stable between different slant angle presentations (**Supplementary Figure 1**).

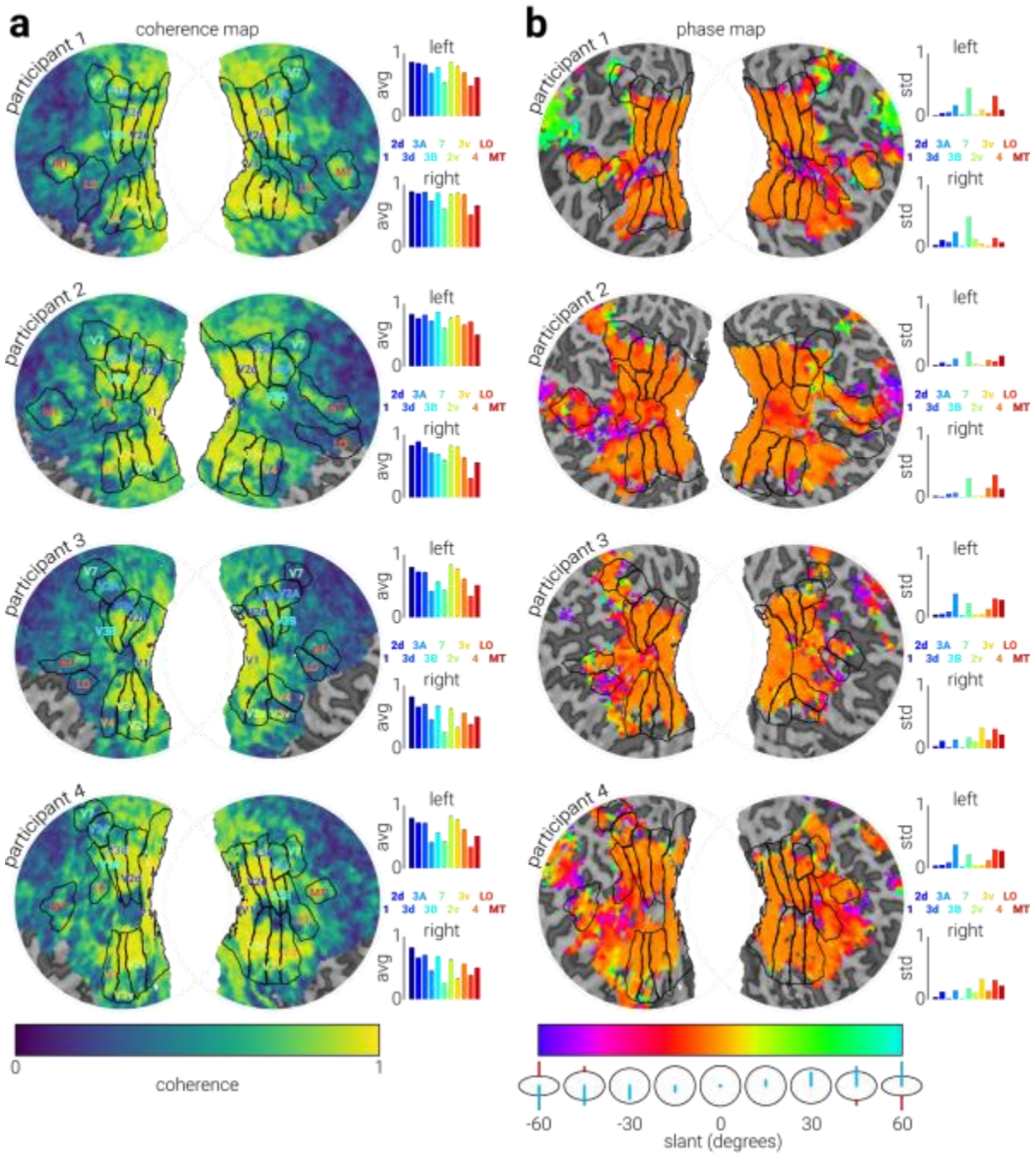

Figure 3. Cortical representation of slant. Slant **a**) coherence and **b**) phase maps for all subjects with retinotopic ROI borders overlaid in black. The plots on the right of the maps show the **a**) average coherence and **b**) standard deviation of phase values within each retinotopic area.

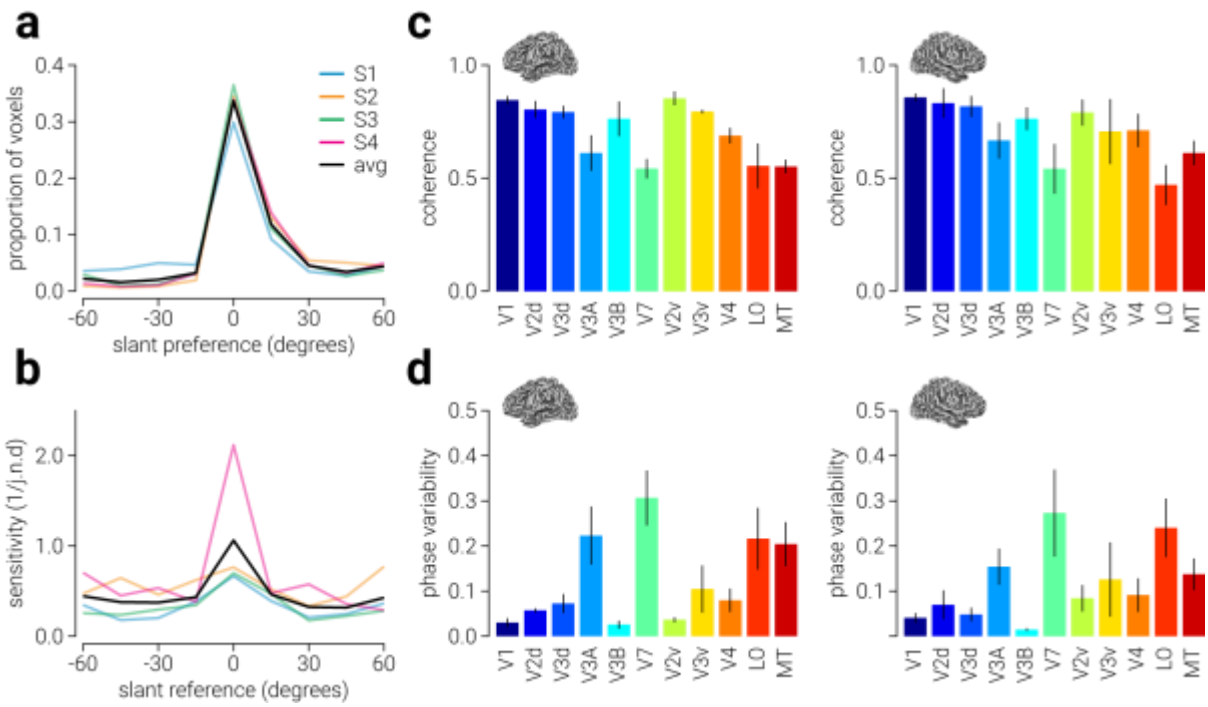

Figure 4. Summary of slant representation. a) The proportion of significant voxels (P<.05) within the recorded region as a function of slant preference. **b**) Slant sensitivity (reciprocal of the just noticeable difference) as a function of the reference slant angle. Colour labels in (**b**) match those in (**a**). (**c-d**) Average (**c**) coherence and (**d**) phase variability within retinotopic areas in the left and right hemisphere across all participants.

Inspection of areas V3A and V7 revealed two types of structure. Participant 1 shows a pattern of slant preference that smoothly transitioned from large negative slant to large positive slant in their right hemisphere, and participant 2 showed an isolated region in which slant preference abruptly changed from negative to positive (**Fig. 5**, broken white lines). However, these structures were not bilaterally present, and we did not observe them in the other participants.

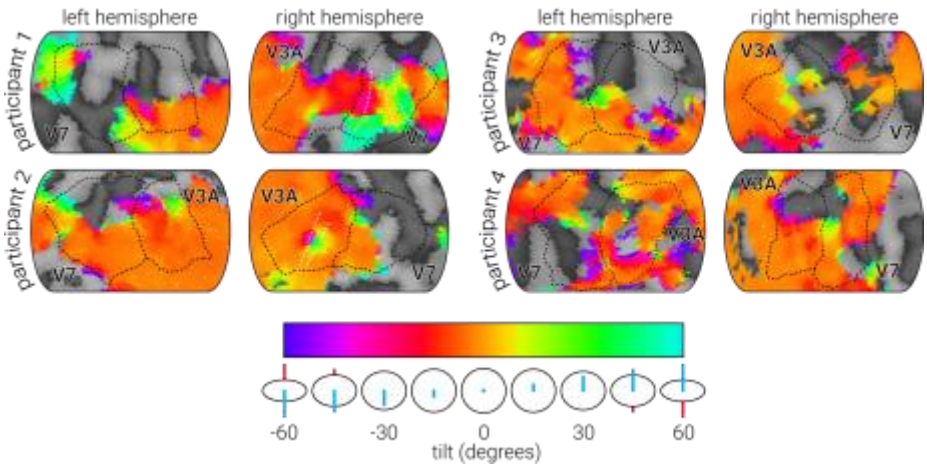

Figure 5. Representation of slant in V3A/V7. Slant phase maps of areas V3A and V7 for all participants. Broken black lines indicate region borders, broken white lines highlight phase transitions.

***Representation of tilt*.** We next measured participants' phase-encoded responses to 3-D tilt from 0-360° at 60° slant, defined by binocular disparity. **Figure 6a** shows the coherence of the activity measured from the visual cortex with the frequency of the travelling wave stimulus. Compared to slant, we found lower coherence values across the visual cortex; however, there was still relatively high coherence within retinoptopically defined visual areas, especially dorsal stream regions, suggesting that the neural populations within these regions were sensitive to aspects of the stimulus which varied as a function of tilt. **Figure 6b** shows the corresponding phase maps for each participant, which were been thresholded to remove phase values with P>.05. Participants 3 and 4 showed a high proportion of phase values corresponding to 0° tilt; however, this was only weakly present in participant 1 and not present in participant 2 (**Fig. 7a**). By contrast, participants showed better performance for cardinal tilt angles than oblique angles (**Fig. 7b**). Assessment of average coherence across visual areas suggested similar levels of coherence (**Fig. 7c**). By contrast, phase variability was highest in V3A and V7, in line with the results from the slant condition (**Fig. 7d**). As in the previous slant condition, we found binocular eye movements were stable between different tilt angle presentations (**Supplementary Figure 2**).

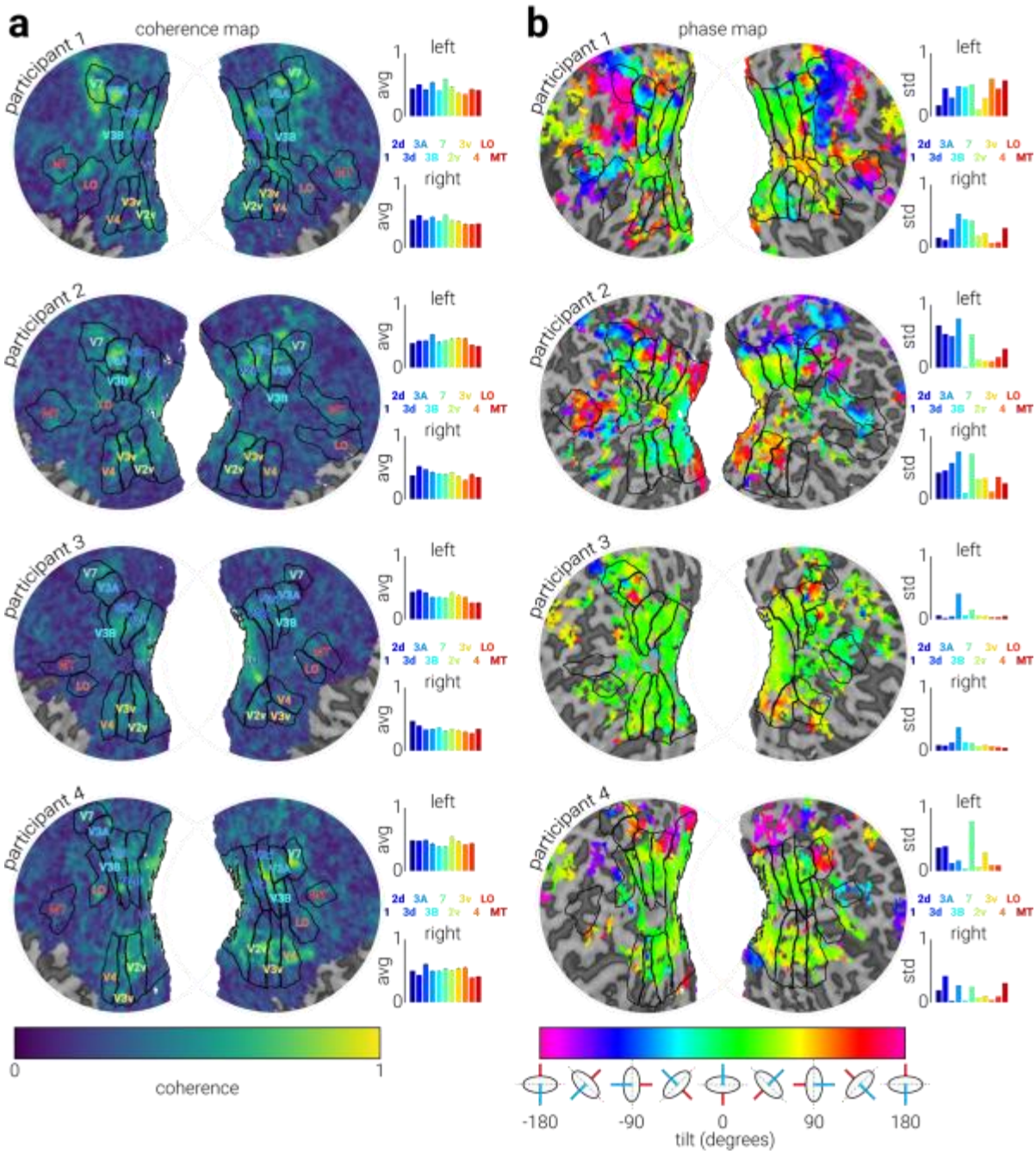

Figure 6. Cortical representation of tilt. Tilt **a**) coherence and **b**) phase maps for all subjects with retinotopic ROI borders overlaid in black. The plots on the right of the maps show the **a**) average coherence and **b**) standard deviation of phase values within each retinotopic area.

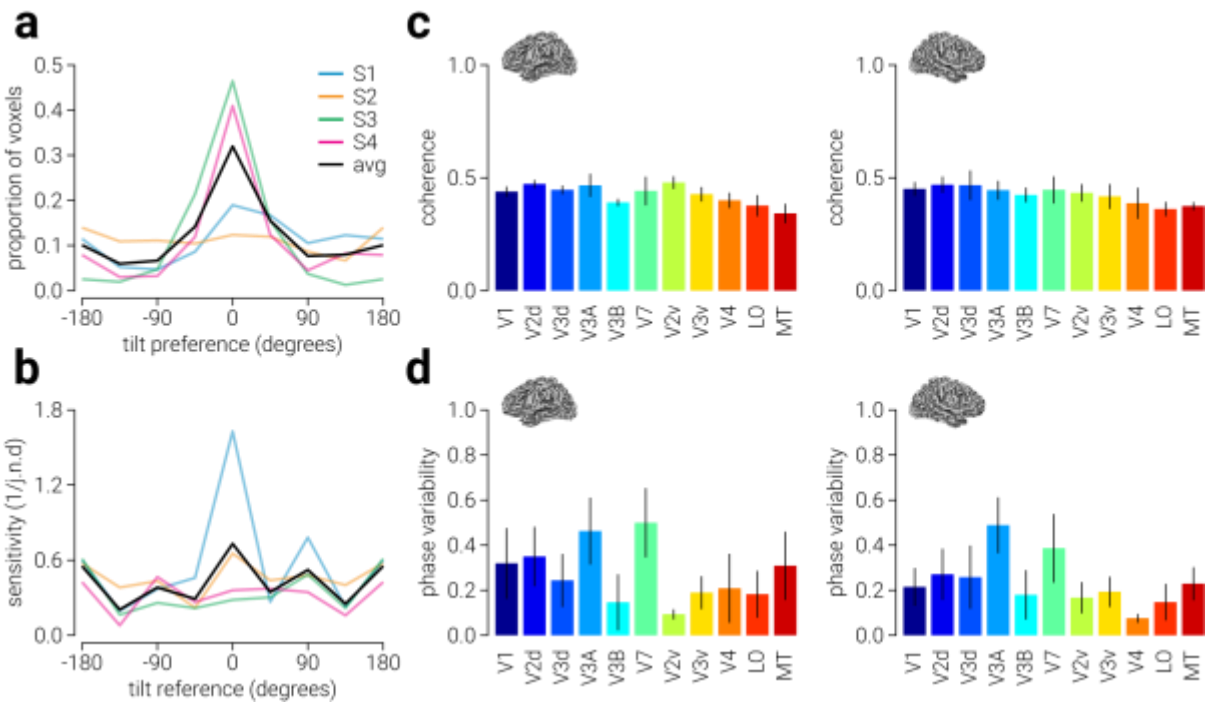

Figure 7. Summary of tilt representation. **a**) The proportion of significant voxels (P<.05) within the recorded region as a function of slant preference. **b**) Tilt sensitivity (reciprocal of the just noticeable difference) as a function of the reference slant angle. Colour labels in (**b**) match those in (**a**). (**c-d**) Average (**c**) coherence and (**d**) phase variability within retinotopic areas in the left and right hemisphere across all participants.

Inspection of areas V3A and V7 revealed two types of structure. Participants 2 and 3 had pinwheel-like structures of tilt preference (**Fig. 8a**, broken white circles); this structure was particularly clear in participant 2 (**Fig. 8b**). Participants 1 and 4 showed abrupt tilt preference reversal, between the border of V3A and V7 (**Fig. 8a**, broken white rectangles). With the exception of participant 1, these structures were not bilaterally present.

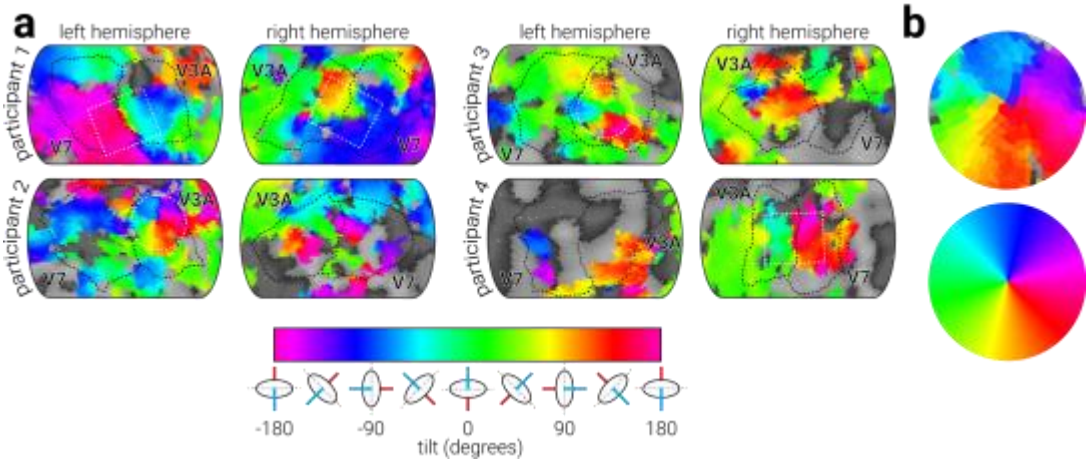

Figure 8. Representation of tilt in V3A/V7. **a**) Tilt phase maps of areas V3A and V7 for all participants. Broken black lines indicate region borders, broken white lines highlight pinwheel formations (circles) and intraregional phase transitions (rectangles). **b**) Comparison of the pinwheel like structure highlighted in the left hemisphere of participant 2 (top) and the tilt phase colour wheel (bottom).

DISCUSSION

Previous fMRI work with humans has identified areas V3A and V7 as responsive to 3-D orientation (Ban & Welchman, 2015; Durand et al., 2009; Georgieva et al., 2009). These studies have employed experimental designs in which conditions are contrasted to reveal activity related to a particular cue. This procedure has been effective in isolating regions that support encoding of 3-D orientation; however, it is blind to any putative functional organization of 3-D orientation selectivity within these areas. Functional organization is likely to be the rule, not the exception, in the brain,as it has the potential to provide computational benefits that arbitrary organization cannot. There are many examples of functional organization within the visual cortex at multiple scales. Classic examples include orientation/ocular dominance columns (Hubel & Wiesel, 1972, 1974) and retinotopic organization (Sereno et al., 1995). In a more recent example, relative depth was shown to be organized in area V3A (Goncalves et al., 2015) in a way that persisted across scan sessions, although no identifiable functional structures were observed. Here we use phase-encoded presentation of planar surfaces with linear gradients of horizontal disparity to test whether the representation of 3-D orientation is functionally organized within the visual cortex. In particular, in two separate sessions we measured fMRI activity of four participants to determine the preference of voxels within the visual cortex for slant angles between ±60° around the x-axis and for tilt angles between 0-360° with 60° slant angle.

For slant we found that frontoparallel (0°) slant was overrepresented within the visual cortex. This is likely a reflection of the distribution of neurons tuned binocular disparity within the visual cortex, which is approximately Gaussian centered on zero disparity (Anzai, Ohzawa, & Freeman, 1999). That is, although we designed the experiment so that even the 0° slant stimuli were offset from the background, the average absolute global disparity was positively related to the slant angle of the stimulus and thus closest to zero for frontoparallel stimuli. Thus, frontoparallel stimuli would have maximally stimulated neurons tuned near-zero binocular disparity, producing a phase-locked pattern of activity consistent with, but misrepresentative of, a preference for frontoparallel slant (this phenomenon likely contributed to the higher coherence values observed in the slant condition than the tilt condition). This result was consistent with the behavioural data, which showed that observers were more sensitive to change in slant around frontoparallel. Despite the overrepresentation of frontoparallel slant preference, we observed two structures in V3A and V7: *i*) participant 1 shows a pattern of slant preference that smoothly transitioned from large negative slant to large positive slant in their right hemisphere, and *ii*) participant 2 showed an isolated region in which slant encoding abruptly changed from negative to positive. However, these structures were not bilaterally present, and we did not observe them in the other participants. One possible explanation for this is that similar structures were obscured in the other participants by the dominant activity evoked by the frontoparallel slant stimuli.

For tilt we also found a nonuniform distribution of tilt preference within the visual cortex, there was a high proportion of voxels which preferred 0° tilt, but this was less pronounced than in the slant condition. Behaviourally, we found that observers were more sensitive to change in tilt angle around the cardinal axes, compared to the oblique. This is consistent with sensitivity to 2-D orientation and motion, which is also best around cardinal axes (i.e., the oblique effect), and likely reflects an anisotropic distribution of 3-D oriented surfaces in the environment. This may partially explain the anisotropic distribution of tilt preference observed. However, the large proportion of voxels that were identified as

preferring 0° tilt may also reflect the anisotropic representation of near and far disparities in the upper and lower visual field. Perceptually, human observers are better at detecting targets defined by crossed (near) disparity (Breitmeyer, Julesz, & Kropfl, 1975) and overestimate the distance of objects in the upper visual field (Ooi, Wu, & He, 2001; Wallach & O'Leary, 1982; Yang & Purves, 2003), while they are better at detecting targets defined by uncrossed (far) disparity and underestimate the distance of objects in the lower visual field (Breitmeyer, Battaglia, & Bridge, 1977). This bias has also been observed physiologically: clustered regions that respond to near and far stimuli are preferentially located in retinotopic regions representing the upper and lower visual fields of V2/3, respectively (Nasr & Tootell, 2018). Although all stimuli in the tilt condition had equal absolute global disparity, the anisotropic representation of near and far disparity in the upper and lower visual field likely resulted in a larger response to the 0° tilt stimuli, thus biasing the distribution of voxel tilt preferences.

We observed two patterns of functional organization of tilt preference in V3A/V7. The first, and perhaps most striking, was a pinwheel-like structure in the left hemisphere of participants 2 and 3. This structure is most clear for participant 2, and encompassed the majority of V3A. Pinwheel-like functional organization has been observed for orientation selectivity in V1 (Blasdel, 1992; Bonhoeffer & Grinvald, 1991). However, the spatial scale of these structures is very different; orientation pinwheels in V1 are ~300 μm in radius, whereas the tilt pinwheels we observed in V3A were ~10 mm in radius. In V1, this structure is thought to bestow at least two benefits for orientation processing: i) preferences for all orientations are brought together, within reach of upper-layer dendrites, and ii) orientation preferences on opposite sides are always perpendicular (Blasdel, 1992). These same benefits may be shared by neurons that encode tilt in V3A; however, as tilt is a vector whose singularities (i.e., the point at the center of the pinwheel) rotate through 360°, tilt angles on opposite sides of the singularity are opposite, as opposed to perpendicular. While the benefits of pinwheel-like functional organization remain an empirical question, patterns resembling this formation that we observe here might suggest that pinwheels are used to represent a different visual property (3-D tilt angle) in a different region (V3A) at a different spatial scale (~30 times larger). While our results are not fully conclusive in that these were not seen across hemispheres or in all participants, they might nevertheless hint that pinwheels represents a canonical organizational structure within the brain.

We found evidence of functional structures that were common to some, but not all participants. It is possible that these structures are not universal; however, it is also possible that we did not detect these structures across all participants due to insufficient resolution and/or signal strength. Future work could build on the findings revealed here by using fMRI at higher field strength (e.g., 7T; Schluppeck, Sanchez-Panchuelo, & Francis, 2018) to target and characterize the representation of slant and tilt in areas V3A and V7. Further, although we used binocular disparity to define the planar surfaces in the current study, V3A and V7 have been shown to respond to 3-D orientation defined by motion (Murray et al., 2003; Orban et al., 1999; Vanduffel et al., 2002), texture (Shikata et al., 2017), and shading (Tsutsui et al., 2001). Thus, future work could compare the representation of 3-D orientation within these areas using different depth cues in isolation and combination.

Using phase-encoded presentation of 3-D stimuli we find evidence in support of the functional organization of 3-D orientation within the visual cortex. In two participants we find fMRI response patterns suggesting that tilt preference is unilaterally organized in a pinwheel-like structure, similar to those observed for orientation preference in V1 (Blasdel, 1992;

Bonhoeffer & Grinvald, 1991), that encompasses most of area V3A. Further, for two participants we find an abrupt reversal in tilt preference reversal at the (retinotopically defined) border between V3A and V7. These findings indicate that 3-D orientation is functionally organized within the human visual cortex, and the discovery of a large pinwheel-like structure suggests that this type of organization may be applied canonically within the brain at multiple scales.

REFERENCES

Anzai, A., Ohzawa, I., & Freeman, R. D. (1999). Neural Mechanisms for Encoding Binocular Disparity: Receptive Field Position Versus Phase. *Journal of Neurophysiology*, *82*(2), 874–890. https://doi.org/10.1152/jn.1999.82.2.874

Backus, B. T., Fleet, D. J., Parker, A. J., & Heeger, D. J. (2001). Human Cortical Activity Correlates With Stereoscopic Depth Perception. *Journal of Neurophysiology*, *86*(4), 2054–2068. https://doi.org/10.1152/jn.2001.86.4.2054

Ban, H., & Welchman, A. E. (2015). fMRI Analysis-by-Synthesis Reveals a Dorsal Hierarchy That Extracts Surface Slant. *Journal of Neuroscience*, *35*(27), 9823–9835. https://doi.org/10.1523/JNEUROSCI.1255-15.2015

Ban, H., Yamamoto, H., Hanakawa, T., Urayama, S. -i., Aso, T., Fukuyama, H., & Ejima, Y. (2013). Topographic Representation of an Occluded Object and the Effects of Spatiotemporal Context in Human Early Visual Areas. *Journal of Neuroscience*, *33*(43), 16992–17007. https://doi.org/10.1523/JNEUROSCI.1455-12.2013

Blasdel, G. G. (1992). Orientation selectivity, preference, and continuity in monkey striate cortex. *The Journal of Neuroscience : The Official Journal of the Society for Neuroscience*, *12*(8), 3139–3161. https://doi.org/10.1523/JNEUROSCI.12-08-03139.1992

Bonhoeffer, T., & Grinvald, A. (1991). Iso-orientation domains in cat visual cortex are arranged in pinwheel-like patterns. *Nature*, *353*(6343), 429–431. https://doi.org/10.1038/353429a0

Brainard, D. H. (1997). The Psychophysics Toolbox. *Spatial Vision*, *10*(4), 433–436. https://doi.org/10.1163/156856897X00357

Breitmeyer, B., Battaglia, F., & Bridge, J. (1977). Existence and Implications of a Tilted Binocular Disparity Space. *Perception*, *6*(2), 161–164. https://doi.org/10.1068/p060161

Breitmeyer, B., Julesz, B., & Kropfl, W. (1975). Dynamic random-dot stereograms reveal up-down anisotropy and left-right isotropy between cortical hemifields. *Science*, *187*(4173), 269–270. https://doi.org/10.1126/science.187.4173.269

DeYoe, E. A., Carman, G. J., Bandettini, P. A., Glickman, S., Wijnen, J. P., Cox, R., … Neitz, J. (1996). Mapping striate and extrastriate visual areas in human cerebral cortex. *Proceedings of the National Academy of Sciences of the United States of America*, *93*(6), 2382–2386. https://doi.org/10.1073/pnas.93.6.2382

Dupont, P., De Bruyn, B., Vandenberghe, R., Rosier, A.-M., Michiels, J., Marchal, G., … Orban, G. A. (1997). The kinetic occipital region in human visual cortex. *Cerebral Cortex*, *7*(3), 283–292. https://doi.org/10.1093/cercor/7.3.283

Durand, J.-B., Peeters, R., Norman, J. F., Todd, J. T., & Orban, G. A. (2009). Parietal regions processing visual 3D shape extracted from disparity. *NeuroImage*, *46*(4), 1114–1126. https://doi.org/10.1016/J.NEUROIMAGE.2009.03.023

Engel, S. A., Rumelhart, D. E., Wandell, B. A., Lee, A. T., Glover, G. H., Chichilnisky, E. J., & Shadlen, M. N. (1994). FMRI of human visual cortex [5]. *Nature*, *369*(6481), 525. https://doi.org/10.1038/369525a0

Georgieva, S., Peeters, R., Kolster, H., Todd, J. T., & Orban, G. A. (2009). The Processing of Three-Dimensional Shape from Disparity in the Human Brain. *Journal of*

Neuroscience, *29*(3), 727–742. https://doi.org/10.1523/JNEUROSCI.4753-08.2009

Goncalves, N. R., Ban, H., Sanchez-Panchuelo, R. M., Francis, S. T., Schluppeck, D., & Welchman, A. E. (2015). 7 Tesla fMRI Reveals Systematic Functional Organization for Binocular Disparity in Dorsal Visual Cortex. *Journal of Neuroscience*, *35*(7), 3056–3072. https://doi.org/10.1523/JNEUROSCI.3047-14.2015

Grill-Spector, K., Kushnir, T., Hendler, T., & Malach, R. (2000). The dynamics of object-selective activation correlate with recognition performance in humans. *Nature Neuroscience*, *3*(8), 837–893. https://doi.org/10.1038/77754

Hubel, D. H., & Wiesel, T. N. (1972). Laminar and columnar distribution of geniculo-cortical fibers in the macaque monkey. *The Journal of Comparative Neurology*, *146*(4), 421–450. https://doi.org/10.1002/cne.901460402

Hubel, D. H., & Wiesel, T. N. (1974). Sequence regularity and geometry of orientation columns in the monkey striate cortex. *Journal of Comparative Neurology*, *158*(3), 267–293. https://doi.org/10.1002/cne.901580304

Kourtzi, Z., Betts, L. R., Sarkheil, P., & Welchman, A. E. (2005). Distributed neural plasticity for shape learning in the human visual cortex. *PLoS Biology*, *3*(7), 1317–1327. https://doi.org/10.1371/journal.pbio.0030204

Murphy, A. P., Ban, H., & Welchman, A. E. (2013). Integration of texture and disparity cues to surface slant in dorsal visual cortex. *Journal of Neurophysiology*, *110*(1), 190–203. https://doi.org/10.1152/jn.01055.2012

Murray, S. O., Olshausen, B. A., & Woods, D. L. (2003). Processing Shape, Motion and Three-dimensional Shape-from-motion in the Human Cortex. *Cerebral Cortex*, *13*(5), 508–516. https://doi.org/10.1093/cercor/13.5.508

Nasr, S., & Tootell, R. B. H. (2018). Visual field biases for near and far stimuli in disparity selective columns in human visual cortex. *NeuroImage*, *168*, 358–365. https://doi.org/10.1016/j.neuroimage.2016.09.012

Neri, P., Bridge, H., & Heeger, D. J. (2004). Stereoscopic Processing of Absolute and Relative Disparity in Human Visual Cortex. *Journal of Neurophysiology*, *92*(3), 1880–1891. https://doi.org/10.1152/jn.01042.2003

Nguyenkim, J. D., & DeAngelis, G. C. (2003). Disparity-based coding of three-dimensional surface orientation by macaque middle temporal neurons. *The Journal of Neuroscience : The Official Journal of the Society for Neuroscience*, *23*(18), 7117–7128. https://doi.org/23/18/7117 [pii]

Ooi, T. L., Wu, B., & He, Z. J. (2001). Distance determined by the angular declination below the horizon. *Nature*, *414*(6860), 197–200. https://doi.org/10.1038/35102562

Orban, G. A., Sunaert, S., Todd, J. T., Van Hecke, P., & Marchal, G. (1999). Human Cortical Regions Involved in Extracting Depth from Motion. *Neuron*, *24*(4), 929–940. https://doi.org/10.1016/S0896-6273(00)81040-5

Pelli, D. G. (1997). The VideoToolbox software for visual psychophysics: Transforming numbers into movies. *Spatial Vision*. https://doi.org/10.1163/156856897X00366

Preston, T. J., Li, S., Kourtzi, Z., & Welchman, A. E. (2008). Multivoxel Pattern Selectivity for Perceptually Relevant Binocular Disparities in the Human Brain. *Journal of Neuroscience*, *28*(44), 11315–11327. https://doi.org/10.1523/JNEUROSCI.2728-08.2008

Rosenberg, A., & Angelaki, D. E. (2014). Gravity Influences the Visual Representation of Object Tilt in Parietal Cortex. *Journal of Neuroscience*, *34*(43), 14170–14180. https://doi.org/10.1523/JNEUROSCI.2030-14.2014

Rosenberg, A., Cowan, N. J., & Angelaki, D. E. (2013). The Visual Representation of 3D Object Orientation in Parietal Cortex. *Journal of Neuroscience*, *33*(49), 19352–19361. https://doi.org/10.1523/JNEUROSCI.3174-13.2013

Schluppeck, D. (2005). Topographic Organization for Delayed Saccades in Human Posterior Parietal Cortex. *Journal of Neurophysiology*, *94*(2), 1372–1384. https://doi.org/10.1152/jn.01290.2004

Schluppeck, D., Sanchez-Panchuelo, R. M., & Francis, S. T. (2018). Exploring structure and function of sensory cortex with 7 T MRI. *NeuroImage*, *164*, 10–17. https://doi.org/10.1016/j.neuroimage.2017.01.081

Sereno, M. I., Dale, A. M., Reppas, J. B., Kwong, K. K., Belliveau, J. W., Brady, T. J., … Tootell, R. B. H. (1995). Borders of multiple visual areas in humans revealed by functional magnetic resonance imaging. *Science*, *268*(5212), 889–893. https://doi.org/10.1126/science.7754376

Shikata, E., Hamzei, F., Glauche, V., Knab, R., Dettmers, C., Weiller, C., & Büchel, C. (2017). Surface Orientation Discrimination Activates Caudal and Anterior Intraparietal Sulcus in Humans: An Event-Related fMRI Study. *Journal of Neurophysiology*, *85*(3), 1309–1314. https://doi.org/10.1152/jn.2001.85.3.1309

Taira, M., Tsutsui, K.-I., Jiang, M., Yara, K., & Sakata, H. (2017). Parietal Neurons Represent Surface Orientation From the Gradient of Binocular Disparity. *Journal of Neurophysiology*, *83*(5), 3140–3146. https://doi.org/10.1152/jn.2000.83.5.3140

Tootell, R. B. H. (2001). Where is “Dorsal V4” in Human Visual Cortex? Retinotopic, Topographic and Functional Evidence. *Cerebral Cortex*, *11*(4), 298–311. https://doi.org/10.1093/cercor/11.4.298

Tsao, D. Y., Vanduffel, W., Sasaki, Y., Fize, D., Knutsen, T. A., Mandeville, J. B., … Tootell, R. B. H. (2003). Stereopsis activates V3A and caudal intraparietal areas in macaques and humans. *Neuron*, *39*(3), 555–568. https://doi.org/10.1016/S0896-6273(03)00459-8

Tsutsui, K.-I., Jiang, M., Yara, K., Sakata, H., & Taira, M. (2001). Integration of perspective and disparity cues in surface-orientation-selective neurons of area CIP. *Journal of Neurophysiology*, *86*(6), 2856–2867. Retrieved from http://www.ncbi.nlm.nih.gov/pubmed/11731542

Tyler, C. W., Likova, L. T., Chen, C.-C., Kontsevich, L. L., Schira, M. M., & Wade, A. R. (2005). Extended Concepts of Occipital Retinotopy. *Current Medical Imaging Reviews*, *1*, 319–329. https://doi.org/10.2174/157340505774574772

Tyler, C. W., Likova, L. T., Kontsevich, L. L., & Wade, A. R. (2006). The specificity of cortical region KO to depth structure. *NeuroImage*, *30*(1), 228–238. https://doi.org/10.1016/j.neuroimage.2005.09.067

Vanduffel, W., Fize, D., Peuskens, H., Denys, K., Sunaert, S., Todd, J. T., & Orban, G. A. (2002). Extracting 3D from motion: Differences in human and monkey intraparietal cortex. *Science*, *298*(5592), 413–415. https://doi.org/10.1126/science.1073574

Wallach, H., & O’Leary, A. (1982). Slope of regard as a distance cue. *Perception & Psychophysics*, *31*(2), 145–148. https://doi.org/10.3758/BF03206214

Wilms, M., Eickhoff, S. B., Hömke, L., Rottschy, C., Kujovic, M., Amunts, K., & Fink, G. R. (2010). Comparison of functional and cytoarchitectonic maps of human visual areas V1, V2, V3d, V3v, and V4(v). *NeuroImage*, *49*(2), 1171–1179. https://doi.org/10.1016/j.neuroimage.2009.09.063

Yang, Z., & Purves, D. (2003). A statistical explanation of visual space. *Nature Neuroscience*, *6*(6), 632–640. https://doi.org/10.1038/nn1059

Zeki, S., Perry, R. J., & Bartels, A. (2003). The processing of kinetic contours in the brain. *Cerebral Cortex*, *13*(2), 189–202. https://doi.org/10.1093/cercor/13.2.189

Zeki, S., Watson, J., Lueck, C., Friston, K., Kennard, C., & Frackowiak, R. (1991). A direct demonstration of functional specialization in human visual cortex. *The Journal of Neuroscience*, *11*(3), 641–649. https://doi.org/10.1523/jneurosci.11-03-00641.1991